Modeling Nanoscale Inhomogeneities for Quantitative HAADF STEM Imaging

Richard Aveyard,[1] Riccardo Ferrando,[2] Roy L. Johnston,[3] and Jun Yuan[1,*]
[1]Department of Physics, University of York, Heslington, York YO10 5DD, United Kingdom
[2]Dipartimento di Fisica, Università di Genova, via Dodecaneso 33, 16146 Genova, Italy
[3]School of Chemistry, University of Birmingham, Edgbaston, Birmingham B15 2TT, United Kingdom
(Received 22 May 2014; published 13 August 2014)

High-angle annular dark-field scanning transmission electron microscopy in conjunction with image simulation is an important tool to determine the structure of nanomaterials. We show that molecular dynamics calculations can be combined with multislice image simulations to account for the large effects of surface-enhanced thermal vibrations and structural relaxation on image intensities. Application to a catalytically important gold cluster shows that the image intensity is sensitive to these surface dominated effects with important implications for three-dimensional structural characterizations.

DOI: 10.1103/PhysRevLett.113.075501 PACS numbers: 61.05.-a, 36.40.Mr, 68.37.Ma

Gold nanoclusters are particularly interesting subjects for study because of the catalytic activity they exhibit, in stark contrast to the noble metal behavior of macroscopic gold. Furthermore, there has been found to be a sharp peak in catalytic turnover in the small multiply twinned regime of clusters with diameters of the order of a few nanometers, the cause of which is yet to be fully understood [1]. While a number of possible theories for this unusual phenomenon have been suggested, a conclusive explanation has yet to be reached [2]. The importance of the geometrical arrangement of the constituent atoms is uncontested, prompting a desire to determine the three-dimensional structures of nanoclusters with atomic precision.

With the recent development of aberration correction, high-angle annular dark-field (HAADF) scanning transmission electron microscopy (STEM) can now regularly achieve subangstrom resolution, making it an ideal candidate for the atomic-resolution characterization of nanoclusters. In this mode, a focused beam of electrons is raster scanned over the surface of the sample. At each incident beam position, the intensity of the beam which is scattered to high angles is recorded so that a map of the sample can be produced. The primary contribution to the high-angle scattering intensity is due to incoherent thermal diffuse scattering, and the signal at the detector is related to the number of atoms in the path of the beam [3,4]. In favorable circumstances, the number of atoms in the direction transverse to the image plane can be deduced from image intensities using statistical parameter estimation methods and used to infer the three-dimensional structure of the specimen [5–7]. In general, however, this approach is inappropriate because of the dynamical scattering of electron beams.

A more precise physical interpretation of the intensities in HAADF STEM images relies upon comparisons between experiments and simulations. To improve the scientific rigor of this approach, LeBeau *et al.* have developed a means by which the HAADF detector system can be calibrated to yield absolute intensity measurements [8]. This allows simulations and experiments to be compared without the use of scaling parameters, which may otherwise conceal valuable information. To capitalize on this development, accurate simulations are required in which all factors affecting image intensities are accounted for. While most artifacts of the microscope can now be measured and accounted for in simulations [9], sample inhomogeneities are often oversimplified. As we shall demonstrate, this can lead to inaccuracies in the structural determination of highly distorted regions, such as at the surfaces of catalytic nanoparticles.

Nanoclusters are inherently strained due to the large proportion of undercoordinated surface atoms which induce atomic reconstruction at the particle surfaces [10]. In addition, gold nanoclusters in the catalytically active size regime often have face centered cubic (fcc) structures with fivefold twinning. The twinning produces clusters with icosahedral and decahedral morphologies, reducing the surface energy. However, the angle between (100) planes is 70.53°, so five perfectly twinned fcc segments only span an angular range of 352.65°, and further lattice distortions are required to close the 7.35° gap [11]. Apart from static structural distortions, the thermal vibrations of atoms in nanocluster structures are also expected to be of greater magnitude than in their bulk counterparts [12]. Both the thermal and static distortions are known to make significant contributions to the image formation process [13,14]. However, difficulties in determining the static distortions with atomic resolution have resulted in the use of regular structures [6]. More significantly, homogeneous bulk Debye-Waller factors are widely applied to nanoscale samples in image simulations [15,16]. As a result, the size-dependent atomic vibration effect has been a concern for quantitative analysis procedures, but no proper treatment has hitherto been applied to the problem.

In this work, a hybrid method is introduced to account for the inhomogeneous structure and thermal vibrations of small metallic nanoclusters in multislice simulations of HAADF STEM images. This is achieved by extracting realistic structure configurations from molecular dynamics simulations for use as models in the frozen phonon algorithm [17]. These structures are inherently distorted by strains and thermal displacements of the atoms from their equilibrium positions. More conventional image simulations have also been performed so that the significance of the effects can be assessed.

Molecular dynamics simulations were performed using the DL_POLY package [18]. The simulations were performed in the microcanonical ensemble to avoid the nonphysical velocity scaling of thermostats. The temperature was approximately controlled by defining the system energy. The atomic interactions were modeled using the semiempirical Gupta potential with parameters taken from Ref. [19]. Crystalline simulations using this potential show similar Debye-Waller factors to those measured experimentally by Peng *et al.*, confirming the suitability of the potential for this work [20]. The prototypical structure for this work is a 284-atom gold nanocluster with a Marks decahedral morphology [21]. This structure has been selected, as it is in the highly catalytic size range, and the Marks decahedron is the favored structure at this size, using the Gupta potential [22]. Before conducting the molecular dynamics simulations, the cluster was structurally relaxed using the conjugate gradient method. The simulation was performed with time steps of 3 fs, an equilibration period of 6 ps, and a production period of 0.9 ns. Configurations were extracted at 30 ps intervals to avoid significant correlations between consecutive structures.

The positions of each atom were recorded at each 3 fs time step throughout the simulation so that the mean square displacement (MSD) of each atom could be calculated. The results are illustrated in Fig. 1, in which each sphere shows the MSD of the atom at that site, multiplied by a factor of 40 to aid visibility.

The mean temperature through the production period of this simulation was 300 ± 10 K. The MSD of the core atom was 0.008 ± 0.001 Å^2, similar to the bulk value at 295 K [20]. The MSDs of the interior atoms increase closer to the surface of the cluster up to 0.012 ± 0.001 Å^2 for the first subsurface layer. The surface atoms exhibit significantly greater MSDs due to their lower coordination with values between 0.019 ± 0.001 Å^2 for the most stable (111) facets and 0.025 ± 0.002 Å^2 for the vertex atoms. These dynamical variations may be catalytically significant for the gold nanoparticles of this size range.

The structural relaxations result in displacements from the equilibrium positions of the atoms, as illustrated in Fig. 2. In atomic column resolved imaging conditions, the high energy beam electrons readily channel into the potential of an atomic column, focusing the beam onto

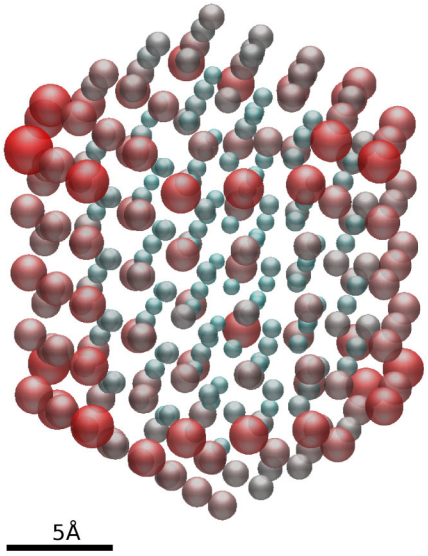

FIG. 1 (color online). Schematic illustrating the variation in mean square displacements at different locations in a 284-atom gold nanocluster. The radii of the spheres are given by the MSD multiplied by a factor of 40.

subsequent atoms and increasing the occurrence of scattering to high angles. Distortions of the column structure, as well as the spacing and number of neighboring columns, affect the extent to which this occurs, and so these factors contribute strongly to the intensities in HAADF STEM imaging [23]. The central nine-atom column of the 284-atom cluster has almost no static displacement transverse to the ⟨110⟩ axis due to its symmetrical location in the cluster. The other columns, however, show barreled distortions, particularly at the surface of the cluster. These distortions may be related to the surface reconstruction seen in larger nanoparticles [10]. The columns lying along the borders of the fivefold symmetry, marked *B* in Fig. 2, exhibit greater curvatures than those of equal atom count in the interior of the fcc segments, labeled *I*, yielding two different types of column for atom counts of six and seven.

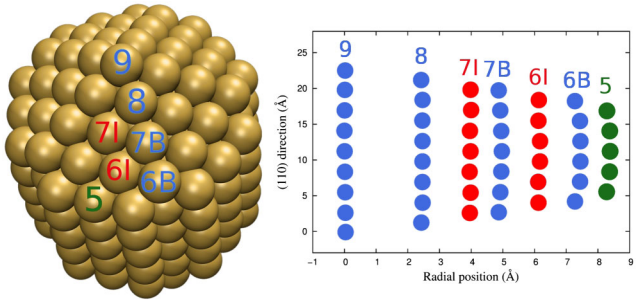

FIG. 2 (color online). Strain-induced displacements of atomic columns transverse to the ⟨110⟩ direction. The labels indicate the number of atoms in the column and whether they lie along the border (*B*) or interior (*I*) of the fcc segments.

Image simulations were performed using a multislice program based on that by Kirkland [24] but modified to utilize the highly parallel architecture of graphics processing units on a workstation computer to reduce computation time. The accuracy of the modified code has been confirmed by comparing images with those produced using Kirkland's unmodified program. The simulations for this work were performed with the cluster oriented so that the ⟨110⟩ zone axis is aligned with the optical axis. The ⟨110⟩ is a shared zone axis for all the fcc segments, so an array of atomic columns is presented to the incident beam. Three multislice HAADF STEM simulations have been performed using different structure models; these are designated *A*, *B*, and *C*. In simulation *A*, a regular model with no structural relaxation was used; thermal vibrations were accounted for using the conventional frozen phonon algorithm with a homogeneous bulk MSD value taken from the literature [20]. In simulation *B*, the mean atomic positions from the molecular dynamics simulation at 300 K were used to reproduce structural relaxations, including surface bond contractions, but the homogeneous bulk MSD value was again applied. In simulation *C*, the frozen phonon algorithm was performed using configurations extracted directly from the molecular dynamics simulation; this provides both structural relaxation and inhomogeneous thermal vibrations. The image simulations were performed for an accelerating voltage of 200 keV, a convergence semiangle of 20 mrad ($k = 0.8$ Å^{-1}), and an annular dark-field detector range of 90 to 230 mrad ($k = 3.6$–9.2 Å^{-1}). The sample was divided into 1.44 Å slices along the beam axis, and 20 frozen phonon configurations were used for each image. The images resulting from these simulations are shown in Fig. 3.

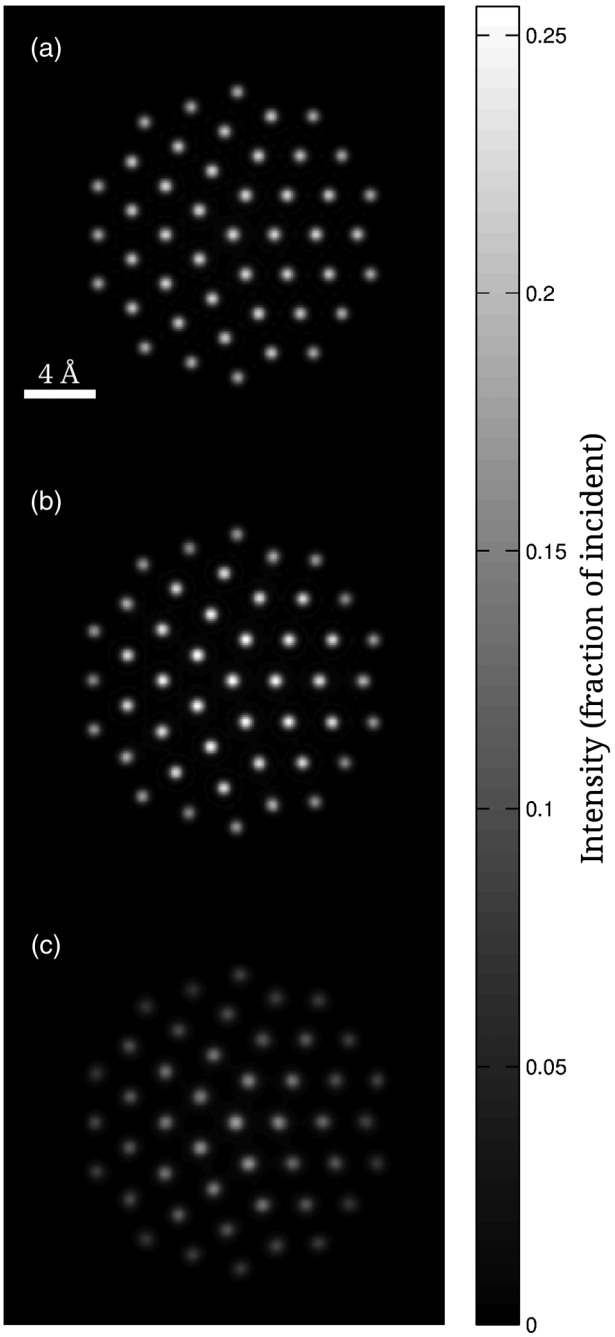

FIG. 3. Simulated HAADF STEM images of a 284-atom gold nanocluster. Simulation *A* used a geometrically regular structure with homogeneous bulk MSDs. Simulation *B* used a relaxed structure with homogeneous bulk MSDs. Simulation *C* used relaxed structures with inhomogeneous thermal vibrations.

To determine the significance of the differences in intensities in images *A*, *B*, and *C*, they should be compared in the same manner in which they would be compared with experimental images. An established quantitative analysis procedure has been applied to each of the images, in which the centers of the intensity peaks are identified and used as sites around which Voronoi cells are generated. The integrated intensity within each cell is then calculated. It has been shown that the integrated column intensity is a robust measurement which changes very little with probe broadening and defocusing [25]. Our own investigation of these two factors confirms this. As the structure used for the simulations is known, the intensity of each spot has been indexed by the number of atoms in the column which produced it; this allows the relationship between atom count and HAADF intensity to be examined. Figure 4 shows the results of this procedure for the three simulations.

The structural relaxation in simulation *B* largely leads to an increase in HAADF intensities relative to those resulting from simulation *A*, in which the perfectly aligned columns have smaller projected scattering cross sections. The exceptions are the five-atom surface columns, which exhibit reduced intensities. These columns are subject to particularly large barrel distortions which attenuate electron channeling sufficiently to cause a reduction in intensities in comparison with the regular model in simulation *A*. The inhomogeneous nature of the structural relaxation can be seen in simulation *B*. As noted previously, columns lying along the twinning borders have greater curvatures than

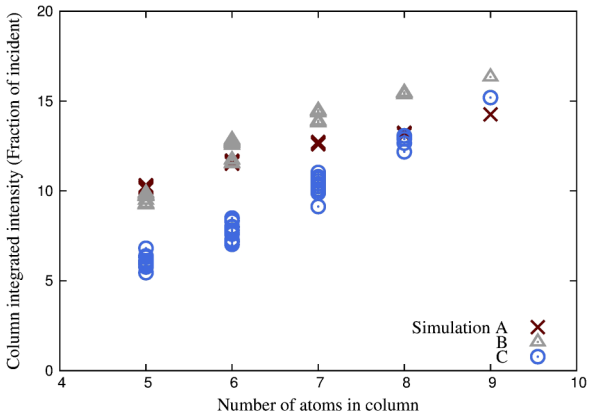

FIG. 4 (color online). Integrated spot intensities from the three simulated images, categorized by the atom count of the column which produced them.

those in the interior. This results in differing intensities for columns containing the same number of atoms, with the better aligned interior columns producing greater HAADF intensities than the curved border columns. This can be seen in both the six- and seven-atom intensities in Fig. 4.

In simulation *C*, atomic coordinates were extracted from molecular dynamics simulations. This gives a similar time-averaged structure to the relaxed model used in simulation *B* but with significantly larger, more realistic thermal vibrations. The increased disorder results in a reduction in the intensities of all the atomic columns, which is attributed to diminished channeling. More specifically, the increased proportion of surface atoms in the shorter columns leads to a greater reduction in their intensities, so that the slope of the column intensity vs atom count increases. This result is consistent with the experimental observation of lower than expected intensities in the outermost columns of a thin gold wedge in Ref. [15], although a lack of accurate structural information precludes a definite attribution to the thermal effects by the authors. A more convincing case is the comparison between the experimental and simulated intensity profiles from HAADF STEM images of a Au_{309} atomic cluster found in Ref. [26], in which the structure is better defined. Close examination of the original paper shows that the slope of the column intensity vs atom count increases more rapidly in the experimental image than in the original simulation profile, which uses the same MSD for all atoms. The application of our hybrid simulation yields a higher slope and is in better agreement with the experiment.

The split intensities of the interior (6*I* and 7*I* in Fig. 2) and border (6*B* and 7*B*) columns observed in simulation *B* are also observed in simulation *C*, although the groupings are less well defined due to the greater spread of intensities caused by the larger thermal vibrations.

It has been demonstrated that size-dependent static and dynamic structural distortions are inhomogeneous and have a strong effect on HAADF STEM image intensities. These effects must be accounted for in order to accurately compare simulations and experiments on an absolute scale. The greater static distortions and the greater thermal vibrations of the columns closer to the surface of the cluster alter the intensity distribution, so normalized comparisons are also susceptible to inaccuracies.

Recently, an analysis method based on statistical parameter estimation procedures has been developed [5,6,27]. In this method, the intensities of spots in zone axis images are collated to produce a data set which is fitted with a number of Gaussian distributions in order to identify statistically significant intensity clusterings. The intensity clusters are assumed to correspond to differing atom counts, and each cluster is assigned an atom count based on a supposed monotonic relationship between atom count and spot intensity. The strain-induced split in the intensity distributions associated with columns of equal atom count but differing curvatures has significant implications for such methods. Application of the technique to the image produced in simulation *C* results in a significant miscount due to the sequential assignment of additional atom counts to both of the two peaks in the two bimodal distributions. While this error would be readily identified by the thermodynamically unlikely structure it produces, this illustrates the limited applicability of the method to strained structures.

The deficiency of the statistical method for such structures can be compensated, if our rigorous and parameter-free simulation is used to provide corrections to the effect caused by the size-dependent static and dynamical distortions. This is relatively straightforward for the symmetrical particles considered here. In the case of the low-symmetry nanoparticles that are often observed experimentally, such calculations can be used in an iterative process in which a trial atomic structure may be obtained using the statistical parameter estimation method or by a reverse Monte Carlo method. Any mistakes in the original structure can be reduced by making structural refinements based on precise comparisons between calibrated experimental images and simulated images, leading to three-dimensional atomic structure determination.

Our hybrid simulation method also opens the way to take into account other dynamical processes, such as knockon damage and subsequent relaxation, either in terms of structural modification or enhanced thermal motion. To compare with our current result, dose-dependent experiments could be performed and results extrapolated back to the zero-dose limit to allow the removal of beam-induced effects. In addition to increasing the accuracy of structural characterizations, the method outlined here could facilitate the measurement of localized dynamic behavior, such as the predicted preferential melting of (100) over (111) surfaces [28].

In conclusion, a hybrid method has been described which allows inhomogeneous structural relaxations and thermal vibrations to be included in dynamic HAADF STEM simulations. As the precise and accurate

interpretation of experimental images is reliant on accurate simulations, these effects must be accounted for in order to correctly characterize samples. Application of this method to a gold nanocluster in the catalytically active size regime produces images which differ in both absolute and relative intensities from those produced using conventional methods, with serious implications for existing structural characterization procedures. The method described here is applicable to any inhomogeneous system for which molecular dynamics and multislice simulations can be accurately performed. With the continuing increase in the availability of computational processing power, the use of such simulations is expected to play an increasingly important role in facilitating the truly quantitative three-dimensional structural study of nanostructures, potentially including the active sites in catalytic systems. Furthermore, our results suggest that in favorable cases, the inhomogeneous distribution of thermal vibrations may be quantifiable, offering insights into local dynamic behavior.

The author would like to thank Dr. A. J. Logsdail, UCL, and Dr. R. F. L. Evans, University of York, for their assistance with the computational work, and Professor Z. Y. Li and Dr. D. S. He for discussions of HAADF STEM operating conditions. This work is supported by EPSRC Grants No. EP/G070474/1 and No. EP/G070326/1 and COST Action MP0903.

*jun.yuan@york.ac.uk

[1] X. Lai and D. W. Goodman, J. Mol. Catal. A: Chem. **162**, 33 (2000).
[2] G. C. Bond, *Gold Nanoparticles for Physics, Chemistry and Biology* (Imperial College Press, London, 2012).
[3] P. D. Nellist and S. J. Pennycook, Ultramicroscopy **78**, 111 (1999).
[4] N. P. Young, Z. Y. Li, Y. Chen, S. Palomba, M. Di Vece, and R. E. Palmer, Phys. Rev. Lett. **101**, 246103 (2008).
[5] S. Van Aert, K. J. Batenburg, M. D. Rossell, R. Erni, and G. Van Tendeloo, Nature (London) **470**, 374 (2011).
[6] D. G. Stroppa, R. D. Righetto, L. A. Montoro, L. Houben, J. Barthel, M. A. L. Cordeiro, E. R. Leite, W. Weng, C. J. Kiely, and A. J. Ramirez, Nanoscale Res. Lett. **8**, 475 (2013).
[7] S. Bals, S. Van Aert, C. P. Romero, K. Lauwaet, M. J. Van Bael, B. Schoeters, B. Partoens, E. Yücelen, P. Lievens, and G. Van Tendeloo, Nat. Commun. **3**, 897 (2012).
[8] J. M. LeBeau, S. D. Findlay, L. J. Allen, and S. Stemmer, Phys. Rev. Lett. **100**, 206101 (2008).
[9] C. Dwyer, C. Maunders, C. L. Zheng, M. Weyland, P. C. Tiemeijer, and J. Etheridge, Appl. Phys. Lett. **100**, 191915 (2012).
[10] M. Mitome, K. Takayanagi, and Y. Tanishiro, Phys. Rev. B **42**, 7238 (1990).
[11] M. J. Walsh, K. Yoshida, A. Kuwabara, M. L. Pay, P. L. Gai, and E. D. Boyes, Nano Lett. **12**, 2027 (2012).
[12] A. Balerna, E. Bernieri, P. Picozzi, A. Reale, S. Santucci, E. Burattini, and S. Mobilio, Phys. Rev. B **31**, 5058 (1985).
[13] D. Van Dyck, Ultramicroscopy **111**, 894 (2011).
[14] V. Grillo, Ultramicroscopy **109**, 1453 (2009).
[15] J. M. LeBeau, S. D. Findlay, L. J. Allen, and S. Stemmer, Nano Lett. **11**, 310 (2011).
[16] S. Van Aert, A. De Backer, G. T. Martinez, B. Goris, S. Bals, G. Van Tendeloo, and A. Rosenauer, Phys. Rev. B **87**, 064107 (2013).
[17] G. Möbus, T. Gemming, and P. Gumbsch, Acta Crystallogr. Sect. A **54**, 83 (1998).
[18] I. T. Todorov, W. Smith, K. Trachenko, and M. T. Dove, J. Mater. Chem. **16**, 1911 (2006).
[19] F. Cleri and V. Rosato, Phys. Rev. B **48**, 22 (1993).
[20] L.-M. Peng, G. Ren, S. L. Dudarev, and M. J. Whelan, Acta Crystallogr. Sect. A **52**, 456 (1996).
[21] L. D. Marks, Rep. Prog. Phys. **57**, 603 (1994).
[22] F. Baletto, R. Ferrando, A. Fortunelli, F. Montalenti, and C. Mottet, J. Chem. Phys. **116**, 3856 (2002).
[23] T. Plamann and M. J. Hÿtch, Ultramicroscopy **78**, 153 (1999).
[24] E. J. Kirkland, *Advanced Computing in Electron Microscopy*, 2nd ed. (Springer, Boston, MA, 2010).
[25] H. E, K. E. Macarthur, T. J. Pennycook, E. Okunishi, A. J. D'Alfonso, N. R. Lugg, L. J. Allen, and P. D. Nellist, Ultramicroscopy **133**, 109 (2013).
[26] Z. Y. Li, N. P. Young, M. Di Vece, S. Palomba, R. E. Palmer, A. L. Bleloch, B. C. Curley, R. L. Johnston, J. Jiang, and J. Yuan, Nature (London) **451**, 46 (2008).
[27] S. Bals, M. Casavola, M. A. van Huis, S. Van Aert, K. J. Batenburg, G. Van Tendeloo, and D. Vanmaekelbergh, Nano Lett. **11**, 3420 (2011).
[28] Y. Wang, S. Teitel, and C. Dellago, Nano Lett. **5**, 2174 (2005).